Protein Engineering of Nitrile Hydratase Activity of Papain: Molecular Dynamics Study of a Mutant and Wild-Type Enzyme

ARTICLE *in* JOURNAL OF THE AMERICAN CHEMICAL SOCIETY · DECEMBER 2002

Impact Factor: 12.11 · DOI: 10.1021/ja020918l · Source: PubMed

4 AUTHORS, INCLUDING:

Swarnalatha Y. Reddy

22 PUBLICATIONS **235** CITATIONS

SEE PROFILE

Yajun Zheng

Vitae Pharmaceuticals

54 PUBLICATIONS **1,361** CITATIONS

SEE PROFILE

J|A|C|S
ARTICLES
Published on Web 10/09/2002

Protein Engineering of Nitrile Hydratase Activity of Papain: Molecular Dynamics Study of a Mutant and Wild-Type Enzyme

Swarnalatha Y. Reddy, Kalju Kahn, Ya-Jun Zheng,† and Thomas C. Bruice*

Contribution from the Department of Chemistry and Biochemistry, University of California−Santa Barbara, Santa Barbara, California 93106

Received July 5, 2002

Abstract: The mechanism of hydrolysis of the nitrile (*N*-acetyl-phenylalanyl-2-amino-propionitrile, **I**) catalyzed by Gln19Glu mutant of papain has been studied by nanosecond molecular dynamics (MD) simulations. MD simulations of the complex of mutant enzyme with **I** and of mutant enzyme covalently attached to both neutral (**II**) and protonated (**III**) thioimidate intermediates were performed. An MD simulation with the wild-type enzyme·**I** complex was undertaken as a reference. The ion pair between protonated His159 and thiolate of Cys25 is coplanar, and the hydrogen bonding interaction $S^-(25)\cdots HD1-ND1(159)$ is observed throughout MD simulation of the mutant enzyme·**I** complex. Such a sustained hydrogen bond is absent in nitrile-bound wild-type papain due to the flexibility of the imidazole ring of His159. The nature of the residue at position 19 plays a critical role in the hydrolysis of the covalent thioimidate intermediate. When position 19 represents Glu, the imidazolium ion of $His159-ND1^+\cdots Cys25-S^-$ ion pair is distant, on average, from the nitrile nitrogen of substrate **I**. Near attack conformers (NACs) have been identified in which $His159-ImH^+$ is positioned to initiate a general acid-catalyzed addition of $Cys-S^-$ to nitrile. Though $Glu19-CO_2H$ is distant from nitrile nitrogen in the mutant·**I** structure, MD simulations of the mutant·**II** covalent adduct finds $Glu19-CO_2H$ hydrogen bonded to the thioimide nitrogen of **II**. This hydrogen bonded species is much less stable than the hydrogen bonded $Glu19-CO_2^-$ with mutant-bound protonated thioimidate (**III**). This observation supports $Glu19-CO_2H$ general acid catalysis of the formation of mutant·**III**. This is the commitment step in the Gln19Glu mutant catalysis of nitrile hydrolysis.

Introduction

Rational design of proteins to carry out desired catalytic roles is a popular endeavor.[1−4] Nitrile compounds are important intermediates in organic synthesis and widely used in the chemical industry and agriculture. Chemical transformations of nitriles require strong acid/base conditions or the use of peroxides. Microbial degradation has been considered as a way to eliminate highly toxic nitriles from industrial waste.[5,6] The two enzymes that commonly catalyze degradation in such microorganisms are nitrile hydratase and nitrilase.[6,7] Nitrile-hydrolyzing enzymes isolated from natural sources are generally rather unstable. Papain is stable under a wide range of conditions of pH and temperature and has been well characterized.[8−12] Papain has been successfully converted into a nitrile hydratase by a single mutation, Gln19Glu in the active site.[13] Due to natural amidase activity of papain, the amide generated from nitrile is further hydrolyzed to the corresponding acid and ammonia. Endowment of papain with nitrile hydratase activity is a fruitful endeavor due to potential use in biotechnological applications.[5−7,14]

The enzyme isolated from papaya latex shares sequence and structural homology with mammalian cysteine proteases. Papain has been used as a model for the structure-based design of inhibitors for cathepsin K and L,[15−16] which are involved in bone degradation in osteoclasts and rheumatoid arthritis. Papain catalyzes the hydrolysis of peptides, amides and esters.[17−19] The hydrolyses of nitrile by papain and natural nitrilase share in

* Author for correspondence. E-mail: tcbruice@bioorganic.ucsb.edu. Phone: 805-893-2044. Fax: 805-893-2229.
† DuPont Agricultural Products, Stine−Haskell Research Center, Newark, DE 19714.

(1) Douglas, K. T. *Curr. Opin. Biotechnol.* **1992**, *3*, 370.
(2) Fersht, A.; Winter, G. *Trends Biochem. Sci.* **1992**, *17*, 292.
(3) Arnold, F. H. *Curr. Opin. Biotechnol.* **1993**, *4*, 450.
(4) Hedstorm, L. *Curr. Opin. Struct. Biol.* **1994**, *4*, 608.
(5) Kobayashi, M.; Shimizu, S. *Curr. Opin. Chem. Biol.* **2000**, *4*, 95; *Nat. Biotechnol.* **1998**, *16*, 733. Yamada, H.; Kobayashi, M. *Biosci. Biotech. Biochem.* **1996**, *60*, 1391.
(6) Kobayashi, M.; Fujiwara, Y.; Goda, M.; Komeda, H.; Shimizu, S. *Proc. Natl. Acad. Sci. U.S.A.* **1997**, *94*, 11986.
(7) Asano, Y.; Tani, Y.; Yamada, H. *Agric. Biol. Chem.* **1980**, *44*, 2251.
(8) Drenth, J.; Jansonius, J. N.; Koekoek, R.; Swen, H. M.; Wolters, B. G. *Nature* **1968**, *218*, 929.
(9) Glazer, A. N.; Smith, E. L. *Enzyme* **1971**, *3*, 501.
(10) Drenth, J.; Jansonius, J. N.; Koekoek, R.; Wolthers, B. G. *Adv. Protein Chem.* **1971**, *25*, 79.
(11) Kamphuis, I. G.; Kalk, K. H.; Swarte, M. B. A.; Drenth, J. *J. Mol. Biol.* **1984**, *179*, 233.
(12) Priestle, J. P.; Ford, G. C.; Glor, M.; Mehler, E. L.; Smith, J. D. G.; Thaller, C.; Jansonius, J. N. *Acta Crystallogr.* **1984**, *A40*, C17.
(13) Dufour, E.; Storer, A. C.; Ménard, R. *Biochemistry* **1995**, *34*, 16382.
(14) Dufour, E.; Wendy, T.; Nagler, K. D.; Storer, A. C.; Ménard, R. *FEBS Lett.* **1998**, *433*, 78.
(15) LaLonde, J. M.; Zhao, B.; Smith, W. W.; Janson, C. A.; DesJarlais, R. L.; Tomaszek, T. A.; Carr, T. J.; Thompson, S. K.; Oh, H.; Yamashita, D. S.; Veber, D. F.; Abdel-Meguid, S. S. *J. Med. Chem.* **1998**, *41*, 4567.
(16) Tsuge, H.; Nishimura, T.; Tada, Y.; Asao, T.; Turk, D.; Turk, V.; Katunuma, N. *Biochem. Biophys. Res. Commun.* **1999**, *266*, 411.
(17) Lowe, G. *Tetrahedron* **1976**, *32*, 291.
(18) Storer, A. C.; Ménard, R. *Methods Enzymol.* **1994**, *244*, 486.
(19) Otto, H.; Schirmeister, T. *Chem. Rev.* **1997**, *97*, 133.

Scheme 1

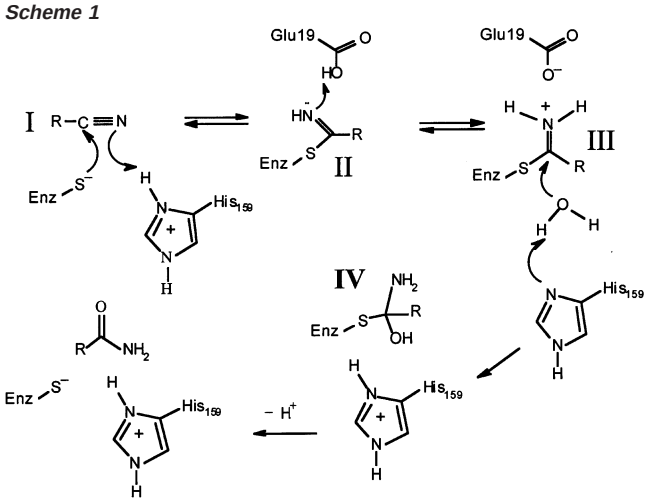

common the participation of cysteine thiolate as a nucleophilic entity.[5] A distinct difference between papain and natural nitrile hydratase is the presence of a metal center in the active site of the latter.[5]

"Peptide nitriles" are reversible inhibitors of papain.[20−23] Nucleophilic attack of the active site cysteine upon nitrile carbon provides a covalent thioimidate. This reaction is endothermic, and the reverse reaction regenerates the nitrile and free enzyme.[24−26] The Gln19Glu mutant papain catalyzes the nitrile hydrolysis with an enhancement of k_{cat} by at least 4×10^5 at pH 5.[13] From ab initio gas-phase calculations, this rate enhancement was attributed by Zheng and Bruice[27] to proton transfer of Glu19−CO_2H to the transition state for general acid catalysis of the formation of the tetrahedral intermediate (**IV** of Scheme 1). It was shown that the differential hydrogen bonding of Glu−CO_2H, as compared to Gln−$CONH_2$, was indeed sufficiently large to account for the observed rate enhancement.[27] As we shall see, proton transfer occurs from Glu−CO_2H to neutral thioimide (**II** of Scheme 1) as proposed by Dufour, Storer, and Ménard.[13]

MD simulations with explicit inclusion of ions and partial mesh Ewald treatment of long-range interactions are likely to provide accurate information about the structural variations and motions of the enzyme complexes. A few MD studies on papain[28−30] and papain-E64 (*N*-[*N*-L-3-trans-carboxyoxirane-2-carbonyl)-L-leucyl]agmatine) complex[31] have been reported. The catalytic mechanism involved in hydrolysis by papain has been explored by semiempirical and quantum mechanical/molecular mechanics (QM/MM) studies.[32−34] Here, we report MD studies

Chart 1

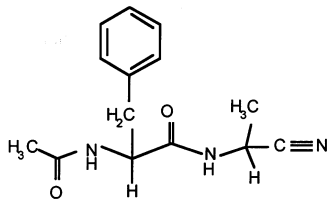

N-acteyl-phenylalanyl-2-amino-propionitrile substrate **I**

on papain and the mutant enzyme (protonated Glu19−CO_2H instead of Gln19−$CONH_2$) complexed to the peptide nitrile substrate, *N*-acetyl-phenylalanyl-2-amino-propionitrile (**I**). In addition, results from simulation of the mutant enzyme covalently bound to the neutral thioimidate (**II**) and protonated thioimidate (**III**) intermediates are discussed.

Methods

Substrate Preparation. The crystal structure (PDB code 6PAD) of papain complexed with inhibitor benzyloxycarbonyl-phenylalanyl-alanyl-chloromethyl ketone (ZPACK)[35] was used as the starting structure. ZPACK was transformed to the corresponding peptide nitrile substrate (*N*-acetyl-phenylalanyl-2-amino-propionitrile, **I**), where the nitrile group is substituted for the terminal −$CO(CH_2)$Cl (Chart 1). The van der Waals and internal parameters of the nitrile group were taken from studies of Howard et al.[36] Atomic charges of nitrile were obtained by means of quantum chemical calculations using Gaussian 98.[37] The fragment O=CH−NH−CH(CH3)−C≡N was optimized at the HF/6-31+G(d,p) level. The electrostatic potential was calculated using the Merz−Singh−Kollman scheme[38] at the MP2/6-31+G(d,p) level. The restrained electrostatic potential (RESP) method[39] was used to fit the electrostatic potential using an atom-centered point charge model. Only the partial charges of the nitrile group were fitted, while the charges of other atoms of that fragment were fixed at the values given in the CHARMM parameter[40] file.

Preparation of Enzyme-Bound Covalent Intermediates. The imine carbon of acetyl-phenylalanyl-2-amino-propiocarboimine and the amine carbon of acetyl-phenylalanyl-2-amino-propiocarboamine were covalently attached to the sulfur atom of Cys25 of mutant papain in enzyme intermediates **II** and **III**, respectively (Chart 2). They were generated from the Cys25 residue of papain using the CHARMM

(20) Lucas, E. C.; Williams, A. *Biochemistry* **1969**, *8*, 5125.
(21) Sluyterman, L. A. E.; Wijdenes, J. *Biochim. Biophys. Acta* **1973**, *302*, 95.
(22) Lewis, C. A., Jr.; Wolfenden, R. *Biochemistry* **1977**, *16*, 4890.
(23) Dufour, E.; Storer, A. C.; Ménard, R. *Biochemistry* **1995**, *34*, 9136.
(24) Brisson, J. R.; Carey, P. R.; Storer, A. C. *J. Biol. Chem.* **1986**, *261*, 9087.
(25) Liang, T. C.; Abeles, R. H. *Arch. Biochem. Biophys.* **1987**, *252*, 626.
(26) Moon, J. B.; Coleman, R. S.; Hanzlik, R. P. *J. Am. Chem. Soc.* **1986**, *108*, 1350. Hanzlik, R. P.; Zygmunt, J.; Moon, J. B. *Biochim. Biophys. Acta* **1990**, *1035*, 62.
(27) Zheng, Y.-J.; Bruice, T. C. *Proc. Natl. Acad. Sci. U.S.A.* **1997**, *94*, 4285.
(28) Wang, J.; Xiang, Y.-F.; Lim, C. *Prot. Eng.* **1994**, *7*, 75.
(29) Swamy, N. K.; Reddy, M. R. *J. Comput. Chem.* **1996**, *17*, 1328.
(30) Drabik, P.; Liwo, A.; Czaplewski, C.; Clarkowski, J. *Prot. Eng.* **2001**, *14*, 747.
(31) Yamamoto, D.; Ohishi, H.; Ishida, T.; Inoue, M.; Sumiya, S.; Kitamura, K. *Chem. Pharm. Bull.* **1990**, *38*, 2339.
(32) Arad, D.; Langridge, R.; Kollman, P. A. *J. Am. Chem. Soc.* **1990**, *112*, 491.
(33) Han, W.-G.; Tajkhorshid, E.; Suhai, S. *J. Biomol. Struct. Dyn.* **1999**, *16*, 1019.
(34) Harrison, M. J.; Burton, N. A.; Hillier, I. H. *J. Am. Chem. Soc.* **1997**, *119*, 12285.
(35) Drenth, J.; Kalk, K. H.; Swen, H. M. *Biochemistry* **1976**, *15*, 3731.
(36) Howard, A. E.; Cieplak, P.; Kollman, P. A. *J. Comput. Chem.* **1995**, *16*, 243.
(37) Frisch, M. J.; Trucks, G. W.; Schlegel, H. B.; Scuseria, G. E.; Robb, M. A.; Cheeseman, J. R.; Zakrzewski, V. G.; Montgomery, J. A., Jr.; Stratmann, R. E.; Burant, J. C.; Dapprich, S.; Millam, J. M.; Daniels, A. D.; Kudin, K. N.; Strain, M. C.; Farkas, O.; Tomasi, J.; Barone, V.; Cossi, M.; Cammi, R.; Mennucci, B.; Pomelli, C.; Adamo, C.; Clifford, S.; Ochterski, J.; Petersson, G. A.; Ayala, P. Y.; Cui, Q.; Morokuma, K.; Malick, D. K.; Rabuck, A. D.; Raghavachari, K.; Foresman, J. B.; Cioslowski, J.; Ortiz, J. V.; Stefanov, B. B.; Liu, G.; Liashenko, A.; Piskorz, P.; Komaromi, I.; Gomperts, R.; Martin, R. L.; Fox, D. J.; Keith, T.; Al-Laham, M. A.; Peng, C. Y.; Nanayakkara, A.; Gonzalez, C.; Challacombe, M.; Gill, P. M. W.; Johnson, B. G.; Chen, W.; Wong, M. W.; Andres, J. L.; Head-Gordon, M.; Replogle, E. S.; Pople, J. A. *Gaussian 98*; Gaussian, Inc.: Pittsburgh, PA, 1998.
(38) Singh, U. C.; Kollman, P. A. *J. Comput. Chem.* **1984**, *5*, 129−145. Besler, B. H.; Merz, K. M.; Kollman, P. A. *J. Comput. Chem.* **1990**, *11*, 431.
(39) Bayly, C. I.; Cieplak, P.; Cornell, W. D.; Kollman, P. A. *J. Phys. Chem.* **1993**, *97*, 10269. Cieplak, P.; Bayly, C. I.; Cornell, W. D.; Kollman, P. A. *J. Comput. Chem.* **1995**, *16*, 1357−1377. Fox, T.; Kollman, P. A. *J. Phys Chem.* **1998**, *102*, 8070.
(40) MacKerell, A. D.; Bashford, D.; Bellott, M.; Dunbrack, Jr.; Evanseck, J. D.; Field, M. J.; Fischer, S.; Gao, J.; Guo, H.; Ha, S.; Joseph-McCarthy, D.; Kuchnir, L.; Kuczera, K.; Lau, F. T. K.; Mattos, C.; Michnick, S.; Ngo, T.; Nguyen, D. T.; Prodhom, B.; Reiher,W. E., III; Roux, B.; Schlenkrich, M.; Smith, J. C.; Stote, R.; Straub, J.; Watanabe, M.; Wiorkiewicz-Kuczera, J.; Yin, D.; Karplus, M. *J. Phys. Chem. B* **1998**, *102*, 3586.

Chart 2.

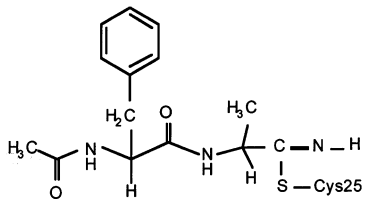

Thioimidate intermediate **II** covalently attached to Cys25 of papain

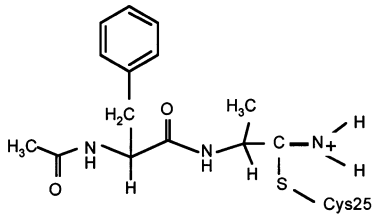

Protonated thioimidate intermediate **III** covalently attached to Cys25 of papain

program.[41] Charge calculations of neutral and protonated thioimidate involved HF/6-31+G(d,p) optimization of O=CH−NH−CH(CH3)−(CH3S)C=NH and O=CH−NH−CH(CH3)−(CH3S)C=NH_2^+ moieties for covalent intermediates **II** and **III**, respectively. RESP fit to the electrostatic potential was evaluated at the MP2/6-31+G(d,p) level. The total charge of the thioimidate intermediate **II** was zero, and that of protonated thioimidate intermediate **III** was +1.

Molecular Simulations. MD Simulations were performed with the program CHARMM[41] (version c27b4) using an all-atom force field.[40] The Leapfrog Verlet integration scheme[42] was used with an integration time step of 1.5 fs. SHAKE[43] was applied to all covalent bonds involving hydrogens. Images were generated using the CRYSTAL module of CHARMM. A constant dielectric of unity was used. Electrostatic interactions were treated with partial mesh Ewald (PME) formalism[44,45] as implemented[46] in the CHARMM program. PME calculations were performed using a real space cutoff of 9 Å with Lennard−Jones interactions truncated at the same distance. A convergence parameter (κ) of 0.32 $Å^{-1}$ and a fifth degree B-spline interpolation were used with the PME method.

The van der Waals parameters and charge of thiolate of Cys25 in the enzyme−substrate complex (**I**) were taken from values reported for methylthiolate in the CHARMM force field.[40] The charge on the C_β atom of Cys25 was adjusted, so that the net charge of the residue was −1. In enzyme complexes (**I**) the imidazole of His159 is protonated at nitogens, while in covalent intermediates (**II**, **III**) His159 has a proton only at the NE2 site. To neutralize the total charge of the enzyme, Cl^- ions were placed at a distance of 3.0 Å near the side chains of solvent-exposed Lys and Arg residues. The enzyme−substrate complexes and enzyme covalent intermediates along with crystal waters were minimized for 100 steps with the steepest descent (SD) and 500 steps with adopted basis Newton−Raphson (ABNR) methods.

Periodic boundary conditions were defined using an orthorhombic box of dimensions (59.79 × 62.94 × 60.07 Å) filled with TIP3P[47] model water molecules. The water molecules in the box were minimized for 100 steps of SD method and equilibrated for a period of 30 ps constant pressure−temperature (NPT) dynamics. Then, the water box was overlaid onto the enzyme−substrate complex or mutant enzyme intermediate with Cl^- ions and crystal waters. Solvent molecules with oxygen atoms within 2.8 Å of any non-hydrogen atoms were deleted. Also, solvent within 3 Å of substrate and 4 Å of Cys25 were removed in papain−nitrile complexes and enzyme covalent intermediates, respectively. The total number of atoms was 23 309 for wild-type, 23 305 for mutant enzyme-nitrile complexes (**I**), 23 305 for **II**, and 23 263 for **III** intermediates. Positions of water molecules were minimized for 100 steps of SD followed by 1000 steps of ABNR methods in each structure, keeping the ions and enzyme complex or covalent intermediate fixed. After that, the entire system was minimized for 1000 steps with the ABNR method before starting simulations.

During the equilibration, the structure was relaxed in stages so that the most strained parts of the system could adjust without introducing artifacts. Initially, a harmonic constraint of force of 100 kcal mol^{-1} $Å^{-1}$ was applied to atoms other than waters and 15 ps simulation was performed at 298 K. Then, the constraints on ions were released and the system was heated gradually from 0 to 298 K, at increments of 10 K, each for 15 ps. Next, all the constraints were removed and the system was reequilibrated by heating the entire model at intervals of 50 K for 15 ps each from 0 to 298 K. These stages were carried out in an NPT ensemble (with a temperature of 298 K and a pressure of 1 atm) so that the water box could equilibrate in accordance with the number of water molecules. The dimensions of the water box were allowed to vary in all directions. During the course of 150 ps, the box dimensions fluctuate by 1−3 Å from the initial values. For subsequent simulations, the constant volume−temperature (NVT) ensemble was used, as it provides more stable trajectories.[48] A 30 ps simulation was run at 298 K, to equilibrate further at this temperature. The heating and equilibration phases of dynamics lasted 180 ps for each of the systems. The production simulation was then continued, at an average temperature of 298 K. The enzyme−substrate (**I**) simulations were performed for a total duration of 1500 ps, while simulations on enzyme covalent intermediates **II** and **III** were carried out for 1000 ps.

Structural Analysis. The root-mean-square deviation (rmsd) values were evaluated by least-squares fitting the backbone heavy atoms of the enzyme to the minimized structure. The positional fluctuations of C_α in the protein backbone were calculated from the MD trajectory, averaged over periods from 451 to 1500 ps in papain−substrate complexes and from 226 to 1000 ps in enzyme covalent intermediates **II** and **III**, respectively. The averaged structure is obtained by least-squares fitting of all the atoms of the complex saved at a 0.75 ps interval from the trajectories to the minimized structure. The experimental positional fluctuations were obtained using the equation $(\Delta r^2)^{1/2} = (3B/8\pi^2)^{1/2}$ from Debye−Waller *B*-factors of papain−cathepsin l-specific inhibitor (CLICK148) complex[16] solved at a 1.7 Å resolution (PDB code 1CVZ).

The averaged structure was minimized for 500 steps of SD for stereo plots, drawn using the programs MOLSCRIPT[49] and Raster3D.[50] Cross correlation between atomic fluctuations were quantified by calculating the covariance between fluctuations of two residues, averaged (for the duration of simulation mentioned above) by residue over C_α atoms of enzyme in each structure.

Results and Discussion

The root-mean-square deviations (rmsd) of the backbone heavy atoms during MD simulations of wild-type and Gln19Glu mutant papain complexes of **I** and enzyme covalent intermediates **II** and **III** (Scheme 1) relative to the minimized crystal structure are shown in Figures 1a and 1b. During the simulation,

(41) Brooks, B. R.; Bruccoleri, R. E.; Olason, B. D.; States, D. J.; Swaminathan, S.; Karplus, M. *J. Comput. Chem.* **1983**, *4*, 187.
(42) Verlet, L. *Phys. Rev.* **1967**, *159*, 98.
(43) Ryckaert, J. P.; Ciccotti, G.; Berendsen, H. J. C. *J. Comput. Phys.* **1977**, *23*, 327.
(44) Darden, T.; York, D.; Pedersen, L. *J. Chem. Phys.* **1993**, *98*, 10089.
(45) Petersen, H. J. *J. Chem. Phys.* **1995**, *103*, 3668.
(46) Feller, S. E.; Pastor, R. W.; Rojnuckarin, A.; Bogusz, S.; Brooks, B. R. *J. Phys Chem.* **1996**, *100*, 17011.
(47) Jorgensen, W.; Chandrasekhar, J.; Madhura, J.; Impey, R.; Klein, M. *J. Chem. Phys.* **1983**, *79*, 926.
(48) Brown, D.; Clarke, J. H. R. *Mol. Phys.* **1984**, *51*, 1243.
(49) Kraulis, P. J. *J. Appl. Crystallogr.* **1991**, *24*, 946.
(50) Merritt, E. A.; Bacon, D. J. *Methods Enzymol.* **1997**, *277*, 505.

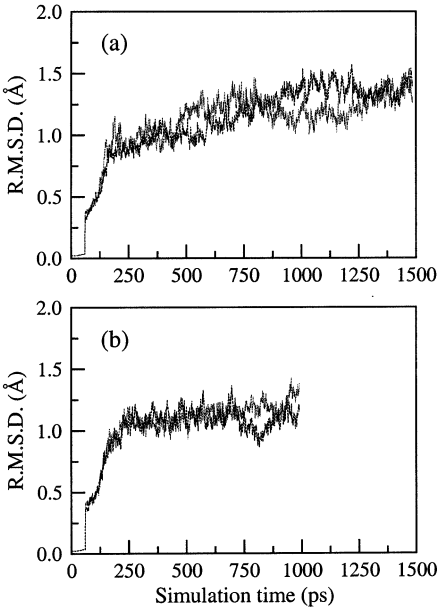

Figure 1. Root-mean-square deviations (rmsd) of the heavy atoms of the backbone of (a) mutant (- - -) and wild-type (····) papain−peptide nitrile complexes, **I**, enzyme covalent (b) thioimidate, **II** (····), and protonated thioimidate, **III** (- - -), intermediates relative to the minimized papain-ZPACK modified crystal structure during simulation.

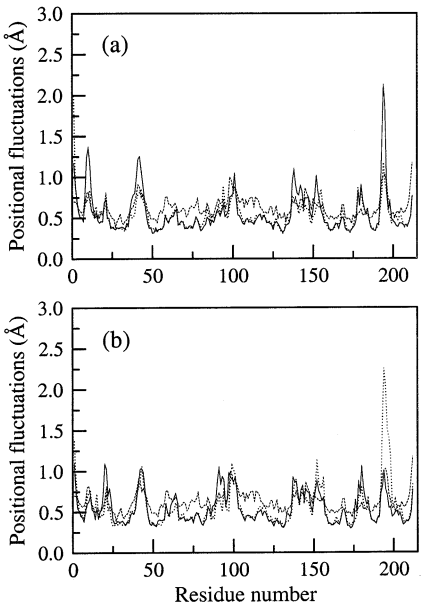

Figure 2. Atomic fluctuations of the C_α atom of the protein backbone of the MD structure of (a) mutant (—) and wild-type (····) papain-nitrile (**I**) complexes averaged for the period from 451 to 1500 ps and enzyme covalent intermediates (b) **II** (····) and **III** (—) averaged for the period from 226 to 1000 ps. Fluctuations of C_α of the papain-CLICK148 crystal structure are also shown in (a) and (b) (- - -).

the rmsd values fluctuate around 1.1−1.45 Å in wild-type·**I** complex and slightly higher values (1.3−1.57 Å) are noticed in mutant enzyme·**I** complex (Figure 1a). Mutant enzyme covalent intermediates **II** and **III** exhibit low values of rmsd; the maxima are 1.37 and 1.36 Å, respectively (Figure 1b). The comparison between positional fluctuations of C_α of the protein backbone evaluated from MD trajectory and crystal structure of papain−CLICK148 complex[16] for all systems are given in Figures 2a and 2b. An examination of Figure 2 indicates that the flexibility noted for the crystal structure is well reproduced over the trajectory, though enhanced motions in coil regions are noticed in the Gln19Glu mutant·**I** complex and covalent intermediate **II**. The helical regions show low amplitude motions.

At neutral pH, the active site of papain contains the Cys25···His159 ion pair.[51−53] The pK_{app} values obtained from the kinetic bell-shaped pH profile have been interpreted as pK_a ≈ 4 for ionization of −SH of Cys25 and pK_a ≈ 8.5 for the protonated imidazole moiety of His159.[19,54] The assignments of Cys−SH and His159−ImH^+ pK_a values have been explained as being due to their presence in the ion pair of Cys25−S^-···His159−ImH^+. The active site lies at the N terminal end of the α-helix formed by residues 24−43. This helix has been proposed to stabilize the Cys25···His159 ion pair.[55] Other residues in and around the active site such as Asp158, Asn175 and Gln19 are in position to form hydrogen bonds either with His159 or the ligand and are important for enzyme activity.[18,56]

Simulation Studies on Mutant Enzyme·I Complex. A stereo diagram of the averaged structure during the period from 451 to 1500 ps of the active site of mutant papain containing **I** is given in Figure 3a. Nonbonded separation between atoms in the active site and the corresponding deviations are given in Table 1.

Orientation of His159 and Associated Conformational Variations. The average distance of 3.28 Å between S^- of Cys25 and ND1 of His159 supports the presence of a persistent ion pair with a hydrogen bond throughout the MD simulation of mutant papain·**I** complex (solid line of Figure 4). The orientation of the His159 flip has been monitored by the change in the dihedral angle $C_\alpha-C_\beta-C_\gamma-C_{\delta 2}$ of His159. For the majority of the simulation time (Figure S1a, Supporting Information), the angle remains at the value required for the Cys25−S^-···His159−$ND1^+$ ion pair (there is a lack of rotation of the imidazole entity). In the averaged position, His159−$ND1^+$ remains in the ion pair but cannot approach and interact with nitrogen (NN) of nitrile (Figure 5a and Table 1).

QM studies and mutagenesis experiments have been offered in support of the proximity of the conserved Asn175 to catalytic His159 to stabilize the ion pair between S^-(Cys25) and ND1(His159).[33,57−58] As seen in Figure S2a (Supporting Information), the solid line indicates that His159 is hydrogen bonded with the amide oxygen, OD1 of Asn175 during the entire MD simulation of mutant papain·**I** complex (see Figure 3 and Table 1). The bond OD1(Asn175)···NE2(His159) is collinear with $C\beta-C\gamma$ of His159, and the associated nonbonded angle OD1-(Asn175)−NE2(His159)−CG(His159) is 155° (solid line of Figure S2b, Supporting Information).

(51) Polgar, L. *FEBS Lett.* **1974**, *47*, 15.
(52) Lewis, S. D.; Johnson, F. A.; Shafer, J. A. *Biochemistry* **1981**, *20*, 48.
(53) Ménard, R.; Carriere, J.; Laflamme, P.; Plouffe, C.; Khouri, H. E.; Vernet, T.; Tessier, D. C.; Thomas, D. Y.; Storer, A. C. *Biochemistry* **1991**, *30*, 8924.
(54) Ménard, R.; Khouri, H. E.; Plouffe, C.; Laflamme, P.; Dupras, R.; Ripoll, D.; Vernet, T.; Tessier, D. C.; Thomas, D. Y.; Storer, A. C. *Biochemistry* **1991**, *30*, 5531.
(55) van Duijnen, P. Th.; Thole, B. Th.; Broer, R.; Nieuwpoort, W. C. *Int. J. Quant. Chem.* **1980**, *17*, 651.
(56) Lavery, R.; Pullman, A.; Wen, Y. K. *Int. J. Quant. Chem.* **1983**, *24*, 353.
(57) Rullmann, J. A. C.; Bellido, M. N.; van Duijnen, P. Th. *J. Mol. Biol.* **1989**, *206*, 101.
(58) Vernet, T.; Tessier, D. C.; Chatellier, J.; Plouffe, C.; Lee, T. S.; Thomas, D. Y.; Storer, A. C.; Ménard, R. *J. Biol. Chem.* **1995**, *270*, 16645.

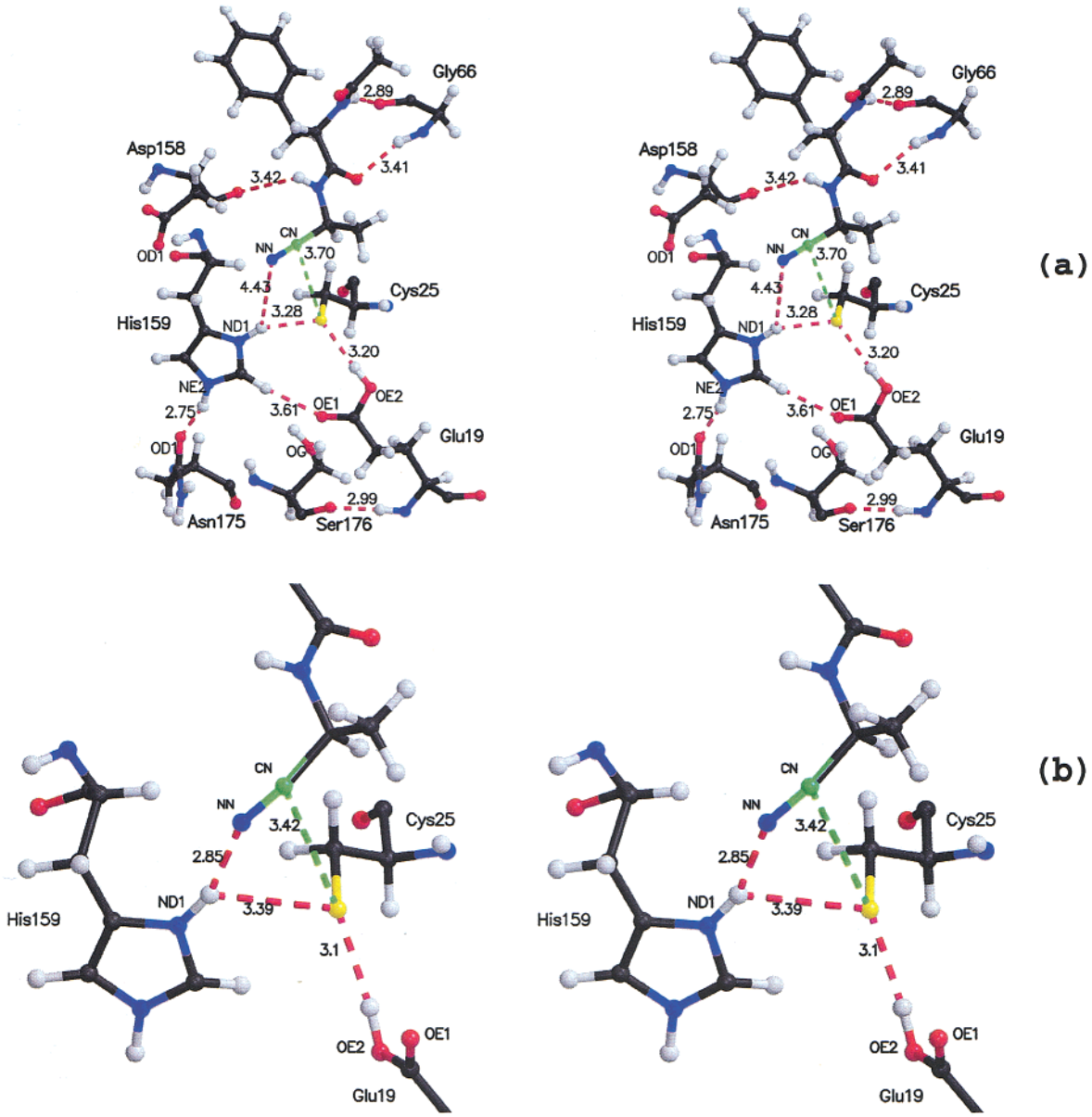

Figure 3. Stereoview of the principal interactions around the active site of the mutant papain·**I** (a) MD structure averaged during the period from 451 to 1500 ps and (b) MD snapshot at 1020 ps satisfying criteria of near attack conformers. The interaction of reactive thiolate with CN of the substrate is shown in green and other nonbonded interactions in red. Average nonbonded distances in Å between heavy atoms are given.

Table 1. Nonbonded Average Distances (Å) and Their Standard Deviations (in Parentheses) of the Active Site of MD Structures of Mutant Papain−Peptide Nitrile Complex and Mutant Enzyme Covalent Intermediates

	mutant papain–nitrile complex		mutant papain thioimidate intermediates	
nonbonded distances	0–405 ps **I**	451–1500 ps **I**	226–1000 ps **II**	226–1000 ps **III**
S(25)···ND1(159)	3.20 (±0.10)	3.28 (±0.21)	3.76 (±0.22)	3.66 (±0.22)
S(25)···CN(substrate)	3.62 (±0.21)	3.70 (±0.22)		
ND1(159)···NN(substrate)/Ni(25)	4.25 (±0.65)	4.43 (±0.64)	4.40 (±0.38)	3.69 (±0.34)
S(25)···OE2(19)	3.28 (±0.18)	3.20 (±0.12)	5.53 (±0.54)	4.02 (±0.14)
OE1(19)···CE1(159)	3.10 (±0.24)	3.61 (±0.71)	3.91 (±0.59)	3.77 (±0.76)
OE2(19)···NN(substrate)/Ni(25)	6.06 (±0.92)	6.68 (±0.32)	3.95 (±0.67)	2.61 (±0.07)
NE2(159)···OD1(175)	2.74 (±0.09)	2.75 (±0.12)	2.89 (±0.16)	3.00 (±0.26)
ND1(159)···OD1(158)	5.69 (±0.33)	5.83 (±0.30)	5.39 (±0.42)	6.76 (±1.02)
O(66)···N(Phe of substrate/25)	2.91 (±0.13)	2.89 (±0.15)	2.88 (±0.14)	3.05 (±0.48)
N(66)···O(Phe of substrate/25)	3.25 (±0.43)	3.41 (±0.42)	2.98 (±0.17)	3.14 (±0.26)
O(158)···N(Ala of substrate/25)	3.21 (±0.43)	3.42 (±0.34)	2.88 (±0.14)	2.89 (±0.14)
N(176)···OD1(175)	2.89 (±0.17)	3.23 (±0.40)	2.82 (±0.15)	2.83 (±0.14)
O(176)···N(19)	2.98 (±0.15)	2.99 (±0.18)	3.16 (±0.27)	2.99 (±0.19)

Nucleophile and Electrophile Interactions. The reaction of papain·**I** complex is initiated by a nucleophilic attack of thiolate of Cys25 on the nitrile carbon (CN) of the substrate (Scheme 1). The distance between the CN carbon atom and S^- of Cys25

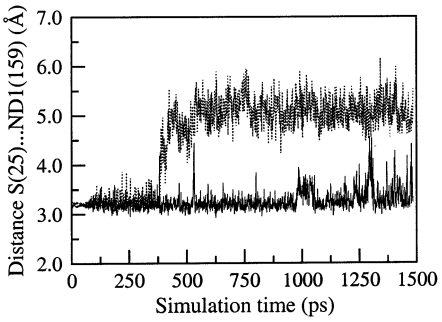

Figure 4. Separation between S(Cys25) and ND1 (His159) for the simulation time from 0 to 1500 ps of mutant (—) and wild-type (····) papain−nitrile **I** complexes.

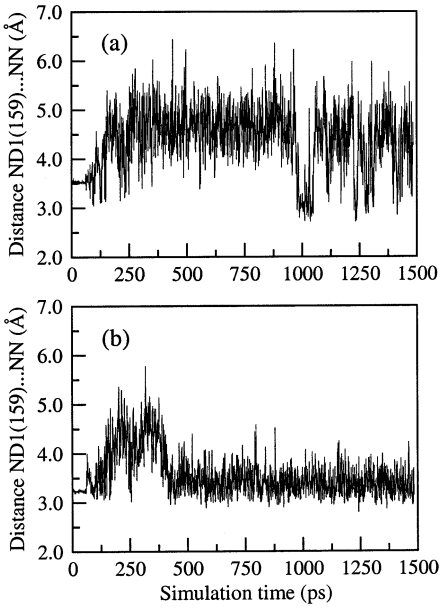

Figure 5. Time-dependent variation of distance between ND1 of His159 and NN of nitrile in (a) mutant and (b) wild-type papain−nitrile **I** complexes.

during the dynamics of mutant enzyme·**I** complex (Figure S3, Supporting Information) averages 3.7 Å, but in a fair number of conformations the distance is less than 3.5 Å, indicating a favorable nonbonded interaction. The near attack conformers (NACs)[59] for Cys25−S^- nucleophilic attack at the nitrile carbon are partially characterized by an approach angle of 90 ± 15° and a Cys25−S^-···CN−NN of <3.5 Å (Figure 6a). Some (31 mol %) mutant·**I** conformers are so characterized. A proton transfer to the nitrile nitrogen must assist the Cys25−S^- nucleophilic addition. His159−$ND1^+$, though at an average distance to the nitrile nitrogen, NN, of 4.2 Å, must be the proton donor. Thus, in addition to an approach angle of 90 ± 15° and a Cys25−S^-···CN−NN of < 3.5 Å, a conformer satisfying NAC criteria requires ND1 of His159 to be in hydrogen bonding distance of NN. The three required distances are present in ∼1.0 mol % of mutant·**I** conformers (Figure 3b).

Conformational Characteristics of Glu19. The $-CO_2H$ side chain of Glu19 forms a hydrogen bond with thiolate of Cys25 with much ease in the mutant papain·**I** complex (solid line of Figure 7a). Also, OE1 of residue 19 is in a position to engage in a favorable interaction with CE1 of His159 in the mutant·**I** complex during most of the simulation time (Figure 7b).

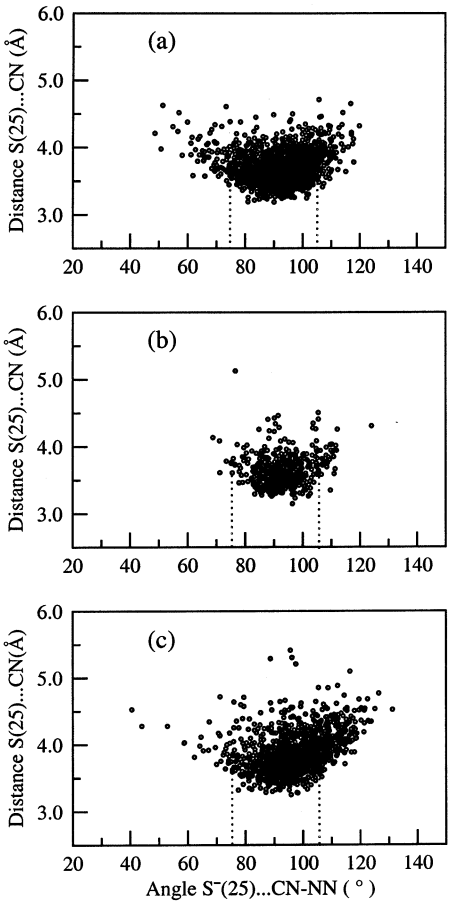

Figure 6. Conformations sampled by angle S(Cys25)···CN−NN and distance S(Cys25)···CN in (a) mutant (0−1500 ps), (b) wild-type (0−450 ps), and (c) wild-type (451−1500 ps) papain−nitrile **I** complexes during MD simulation. Structures within the dashed lines have near attack conformational criteria.

It should be noted that in the averaged MD structure, Glu19−CO_2H is not in the vicinity of the nitrile in the mutant enzyme·**I** complex.

Other Conformational Variations. Noteworthy are certain conformational features around the active site of mutant papain complex of **I** (Table 1). The amide nitrogen and carbonyl oxygen of Gly66 are hydrogen bonded to the carbonyl oxygen and amide nitrogen, respectively, of the Phe residue of **I**. The carbonyl oxygen of Asp158 is hydrogen bonded to the amide nitrogen that is proximal to the nitrile group of **I** (Figure 3a). The carbonyl oxygen of Ser176 forms a hydrogen bond with the backbone amide of residue 19 in mutant·**I** complex (Figure 3a and Table 1).

Simulation Studies on Wild-Type Papain·I Complex and Comparison with Mutant Enzyme·I Complex. An examination of Figure 8a and Table 2 indicates that the conformational features observed in wild-type papain·**I** complex averaged for the period from 0 to 405 ps are similar to those observed in the MD structure of mutant enzyme·**I** complex. An abrupt change in the active site of the wild-type papain·**I** structure is observed at ∼405 ps. From 451 to 1500 ps, the MD structures of wild-type and mutant complexes of **I** differ. Another MD simulation performed on wild-type papain·**I** complex with a different starting structure (MD conformer at 305 ps) for 1 ns also showed similar changes at ∼405 ps. In what follows, we discuss the

(59) Lightstone, F. C.; Bruice, T. C. *J. Am. Chem. Soc.* **1996**, *118*, 2595.

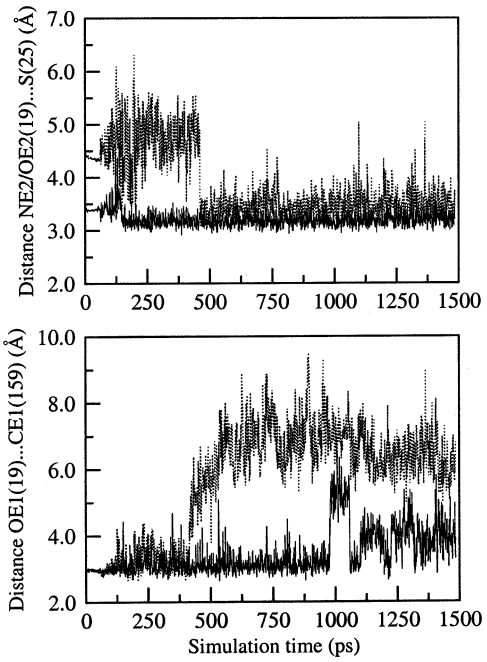

Figure 7. Time-dependent variation of (a) NE2(19)/OE2(19)···S(Cys25) and (b) OE1(19)···CE1(His159) in mutant (—) and wild-type (····) papain−peptide nitrile **I** complexes.

differences and similarities of wild-type papain·**I** complex with respect to mutant papain·**I** complex.

MD Averaged (451−1500 ps) Structure of Wild-Type Papain·I Complex. Orientation of His159 and Associated Conformational Variations. It is assumed that in the free form of papain, the ion pair thiolate of Cys25 and ND1 of His159 is coplanar.[35] The planarity of Cys25···His159 ion pair is disrupted upon the binding of ordinary peptide substrates.[33,35,60] In our MD simulation studies, the orientation of His159 side chain changes in the wild-type papain·**I** complex at ∼405 ps. This results in the disruption of the hydrogen bond interaction between Cys25−S^- and His159−$ND1^+$ seen in Figure 4 (dotted line). The imidazole ring of His159 rotates away (flipping motion) from the thiolate of Cys25 (see Figure 8b).

His159−ImH^+ has been suggested to be the required proton source in the mechanism of papain catalysis.[33,35] The flip of a ∼30° increment in the dihedral angle $C_\alpha-C_\beta-C_\gamma-C_{\delta 2}$ of His159, in the time-averaged MD structure, is seen in Figure S1b, Supporting Information. In this turned orientation, the imidazolium moiety ND1 of His159 is, on average, 3.4 Å from the NN atom of nitrile (Figure 5b and Table 2). However, the ND1 points away from **I** such that in this conformation, the ND1 of imidazole cannot donate the proton and assist thioimidate (**II**) formation.

In the conformational change at 405 ps, the nonbonded angle, OD1(Asn175)−NE2(His159)−CG(His159) changes from 155 to 70° (dotted line of Figure S2b, Supporting Information). Associated conformational changes are hydrogen bond breaking between His159 and Asn175 (Figure S2a, Supporting Information). In place, ND1 of His159 is at 2.6 Å from the carboxylate oxygen of Asp158−CO_2^-, indicating a hydrogen bond between these two entities (Figure S2c, Supporting Information and Table 2). These features are depicted in the averaged coordinates of MD simulated wild-type papain·**I** complex (Figure 8). The motions of His159 are consistent with cryoenzymological reports about conformational changes during the reaction[61] and also with the proposal of the significant role of the hydrogen bonding interactions involving the Asp158 side chain.[54] The switchover of hydrogen bond formation seen in the wild-type papain·**I** complex (Figure 7) has been observed in a previous MD study on papain.[28]

Conformational Characteristics of Gln19. There is hydrogen bonding between Cys25−S^- and the terminal amide −NH2 of the Gln19 enzyme (dotted line of Figure 7a), while the CE1−HE1(His159)···OE1(Gln19) interaction is no longer observed (Figure 7b). In its place, OE1 of Gln19 is hydrogen bonded to OH of Ser176 (Figure 8b). A strong hydrogen bond is observed between OD1 of Asn175 and the backbone amide of Ser176, while such an interaction fluctuates widely in the mutant enzyme·**I** complex (Table 2).

Similarities between Wild-Type and Mutant Papain·I Complex after 450 ps. Nucleophile and Electrophile Interactions. The distance between the −CN carbon atom of **I** and Cys25−S^- during dynamics (dotted line of Figure S3, Supporting Information) is, on average, ∼3.86 Å in wild-type enzyme·**I** complex. From plots of angle Cys25−S^-···CN−NN versus the nonbonded distance S^-···CN (Figure 6), it is obvious that the hydrogen bonding interaction S^-(Cys25)···HD1−ND1-(His159) is mainly independent of the separation between nucleophile and electrophile in the wild-type enzyme·**I** complex. Reactive NACs based on the attack angle of Cys25−S^- on the nitrile of **I** are identified in a similar way as that of mutant enzyme·**I** complex. Conformations possessing the geometry of **I** and Cys25−S^- required for a NAC represent 13 mol % of the total ground state conformers. This value is less than those observed before 405 ps with 48, and 31 mol % with mutant·**I** complex (Figure 6). Similar other conformational variations discussed with mutant·**I** complex are also observed here.

Simulation Studies on Mutant Enzyme Covalent Intermediates II and III (Scheme 1). Most of the interactions observed around the active site of mutant papain·**I** complex are observed in structures of mutant covalent thioimidate (mutant·**II**) and protonated thioimidate (mutant·**III**) intermediates (Table 1). However, upon addition of thiolate to nitrile accompanied by protonation of the nitrile nitrogen by His159−ImH^+, there is a major change in reactant conformation. This can be seen in the comparison of structures of mutant·**I** (Figure 3a), mutant·**II**, and mutant·**III** (Figure 9). The ion pair of His159−$ND1^+$···Cys25−S^- must separate in order to offer a proton to the nitrile nitrogen and initiate nucleophilic addition of Cys25−S^- to **I**. This process is accompanied by the movement of the thioimidate (**II**) intermediate deeper into the active site. This motion allows the proton of Glu19−CO_2H to be at a hydrogen bonding distance to the imino nitrogen (Ni) of neutral thioimidate intermediate **II**.

The carboxylic acid entity of Glu19 is adjacent to the thioimidate in the mutant·**II** complex. The endergonic thioimidate (**II**) covalent intermediate of papain is unstable and reverts to **I**. This is because any hydrogen bonding of the Gln19−$CONH_2$ to **II** would be ineffectual in the stabilization of the latter.[27] By protonation of **II**, the presence of Glu19−CO_2H leads to hydrolysis of the nitrile and, consequently, to accumula-

(60) Turk, B.; Turk, V.; Turk, D. *Biol. Chem.* **1997**, *378*, 141.

(61) Angelides, K. J.; Fink, A. L. *Biochemistry* **1979**, *18*, 2363.

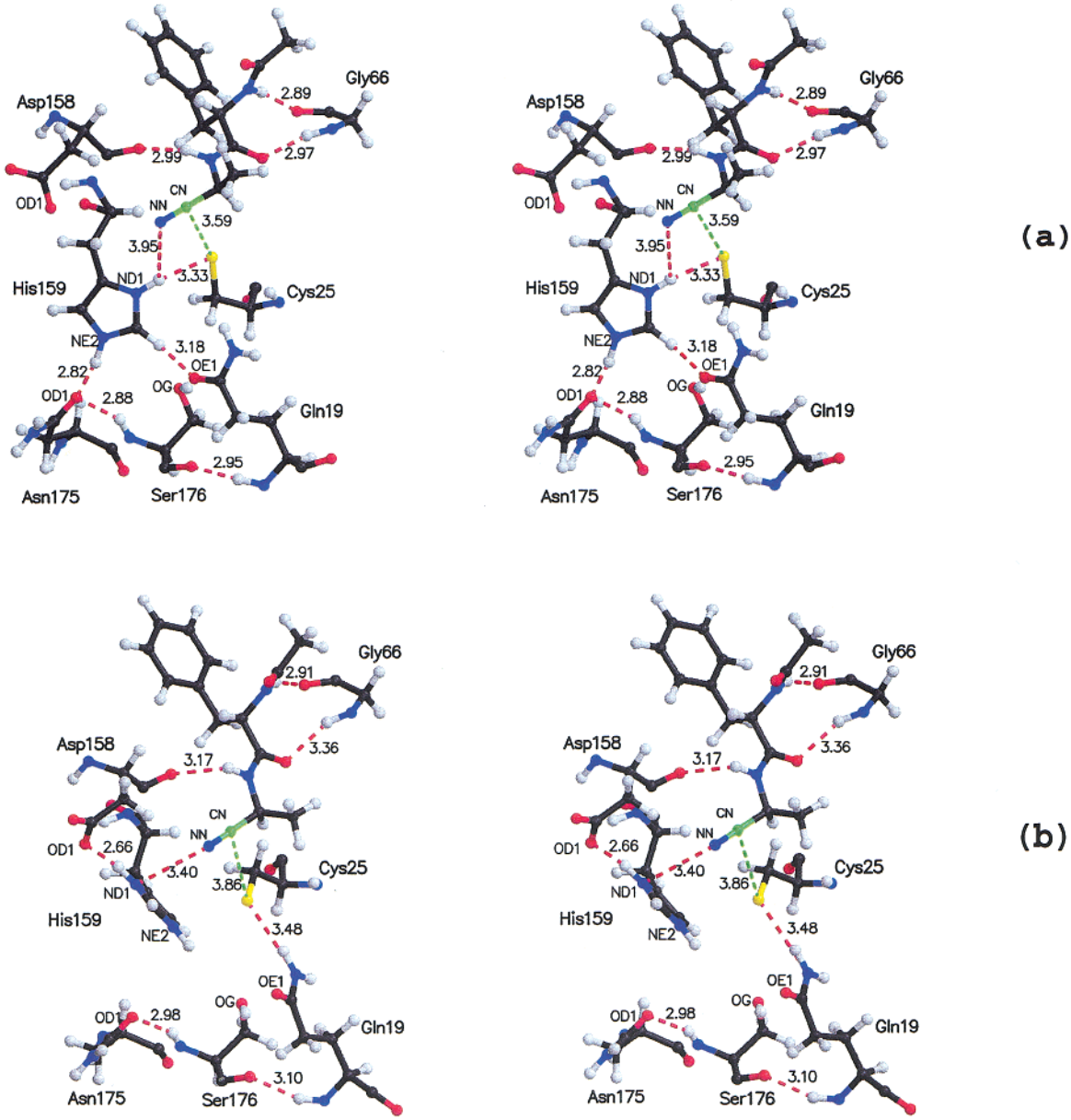

Figure 8. Stereoview of the active site of wild-type papain·**I** MD structure averaged for periods (a) from 0 to 405 ps and (b) from 451 to 1500 ps. Notice the flip of the imidazole ring of His159 in b. Average nonbonded distances in Å between heavy atoms are given.

Table 2. Nonbonded Average Distances (Å) and Their Standard Deviations (in Parentheses) of the Active Site of MD Structures of the Wild-Type Papain−Peptide Nitrile Complex

	wild-type papain–nitrile complex	
nonbonded distances	0–405 ps **I**	451–1500 ps **I**
S(25)···ND1(159)	3.33 (±0.27)	5.07 (±0.28)
S(25)···CN(substrate)	3.59 (±0.23)	3.86 (±0.30)
ND1(159)···NN(substrate)	3.95 (±0.57)	3.40 (±0.24)
S(25)···NE2(19)	4.65 (±0.43)	3.48 (±0.24)
OE1(19)···CE1(159)	3.18 (±0.33)	6.63 (±0.73)
NE2(19)···NN(substrate)	5.28 (±1.05)	6.88 (±0.48)
NE2(159)···OD1(175)	2.82 (±0.22)	6.39 (±0.40)
ND1(159)···OD1(158)	5.56 (±0.40)	2.66 (±0.09)
O(66)···N(Phe of substrate)	2.89 (±0.13)	2.91 (±0.15)
N(66)···O(Phe of substrate)	2.97 (±0.15)	3.36 (±0.46)
O(158)···N(Ala of substrate)	2.99 (±0.29)	3.17 (±0.31)
N(176)···OD1(175)	2.88 (±0.16)	2.98 (±0.24)
O(176)···N(19)	2.95 (±0.14)	3.10 (±0.33)

tion of the corresponding amide, which is further slowly hydrolyzed to the acid by the mutant papain.

In the mutant enzyme **II** intermediate structure, Ni of thioimidate is hydrogen bonded to the carboxylic acid OE2 of Glu19. This hydrogen bond fluctuates widely (dotted line in Figure 10). Transfer of the Glu19−CO_2H proton to intermediate **II** provides the hydrogen bonding of Glu19−CO_2^- to the thioimide nitrogen of **III**, which is thermodynamically favorable (Chart 3). Thus, MD simulation of mutant·**III** intermediate supports a stable hydrogen bond between the OE2 of Glu19 carboxylate and one of the amide hydrogens of **III** (solid line of Figure 10). This proton-transfer prevents return of **II** to **I** plus Cys25−S^-. Conformers identified within 3.0 Å separations of Glu19−CO_2H and Ni of thioimide of **II** are at 10 mol % mutant·**II** intermediate, and one of them is shown in Figure 9b. The protonated thioimidate intermediate **III** is susceptible to nucleophilic attack by a water molecule. The latter reaction is likely to be assisted by His159 general base catalysis (**IV** of Scheme 1). Distinctly one or the other TIP3P water is proximal

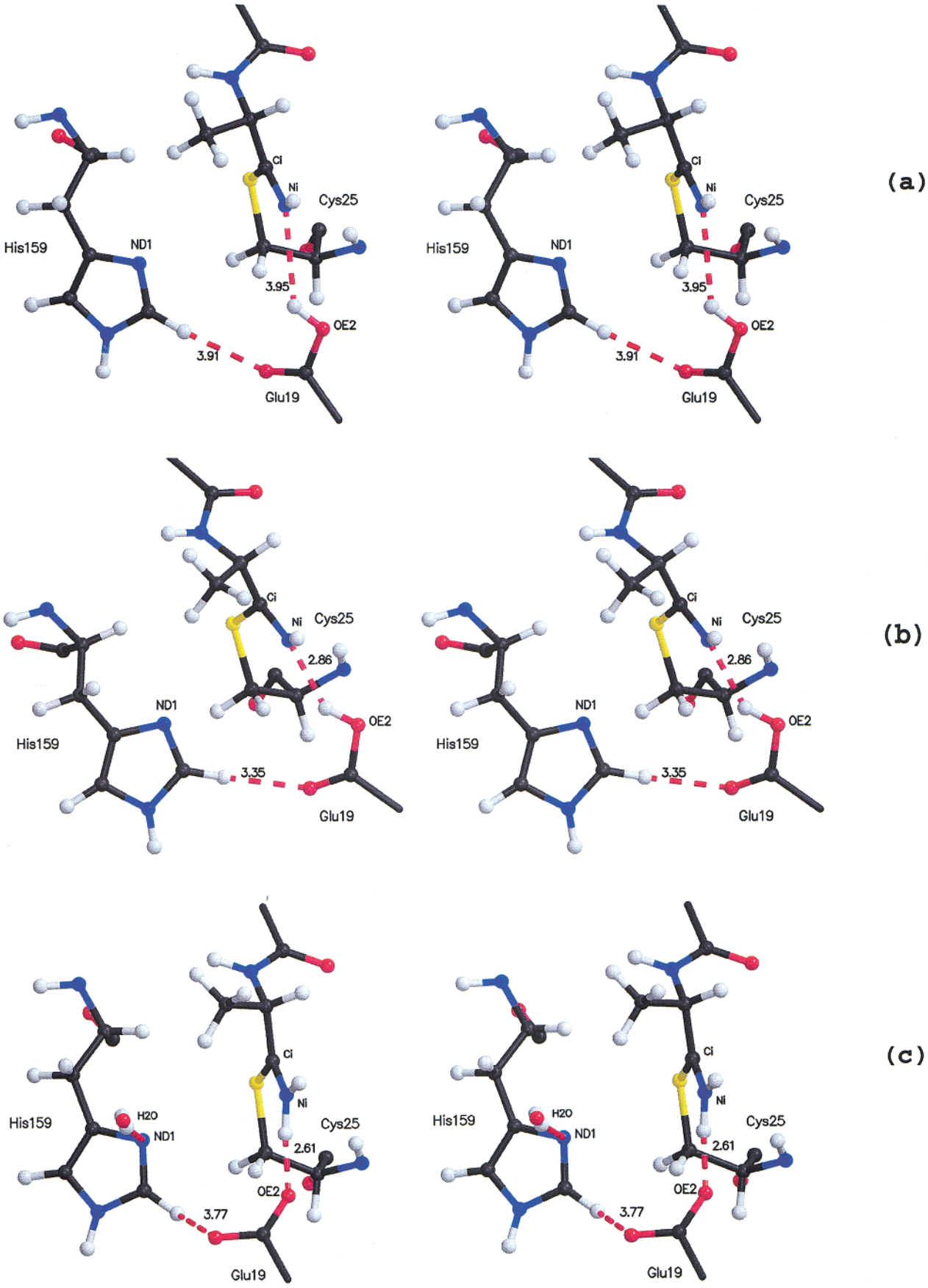

Figure 9. Stereodiagrams of the principal interactions around the active site of MD structures of mutant papain (a) thioimidate intermediate **II**, averaged for 226−1000 ps; (b) MD snapshot of **II** at 924 ps satisfying NAC criteria; and (c) protonated thioimidate intermediate **III**, averaged for 226−1000 ps. Average nonbonded distances in Å between heavy atoms are given.

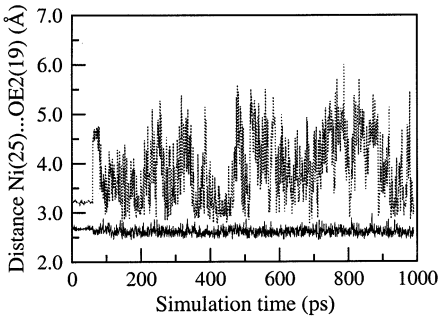

Figure 10. Distance variation with time for the hydrogen bond between Glu19-COOH···Ni(H)═C(R)−S−Cys25 of thioimidate **II** (····) and Glu19-COO^{-}···HNi(H)═C(R)−S−Cys25 of protonated thioimidate **III** (—).

to ND1 of His159 to form a strong hydrogen bond during the entire simulation (Figure 9c).

Correlated and Anticorrelated Motions. An overview of cross-correlation between atomic fluctuations provides insight into correlated, anticorrelated, and uncorrelated motions in the enzyme. Such an analysis (performed after 450 ps of papain·**I** complexes and after 225 ps of mutant enzyme covalent intermediates), shown in Figure 11, gives valuable information about the whole protein environment and interactions of the active site. The positive correlations occur among residues that are either part of the secondary structure element or at the interface of secondary and tertiary enzyme−substrate complexes (Figures 12a and 12b). The polypeptide chain of papain has 212 amino acids and forms two domains, R (residues 1−9 and 109−206) and L (residues 10−108 and 207−212).[10,11] α-Helices predominate in L, while β-barrel motifs abound in R (see Figure 12). A few extended positive correlations observed in the mutant

Chart 3

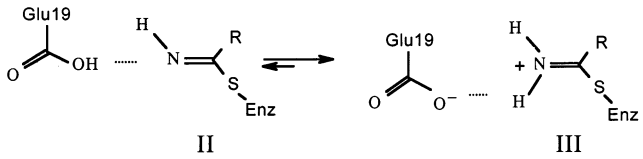

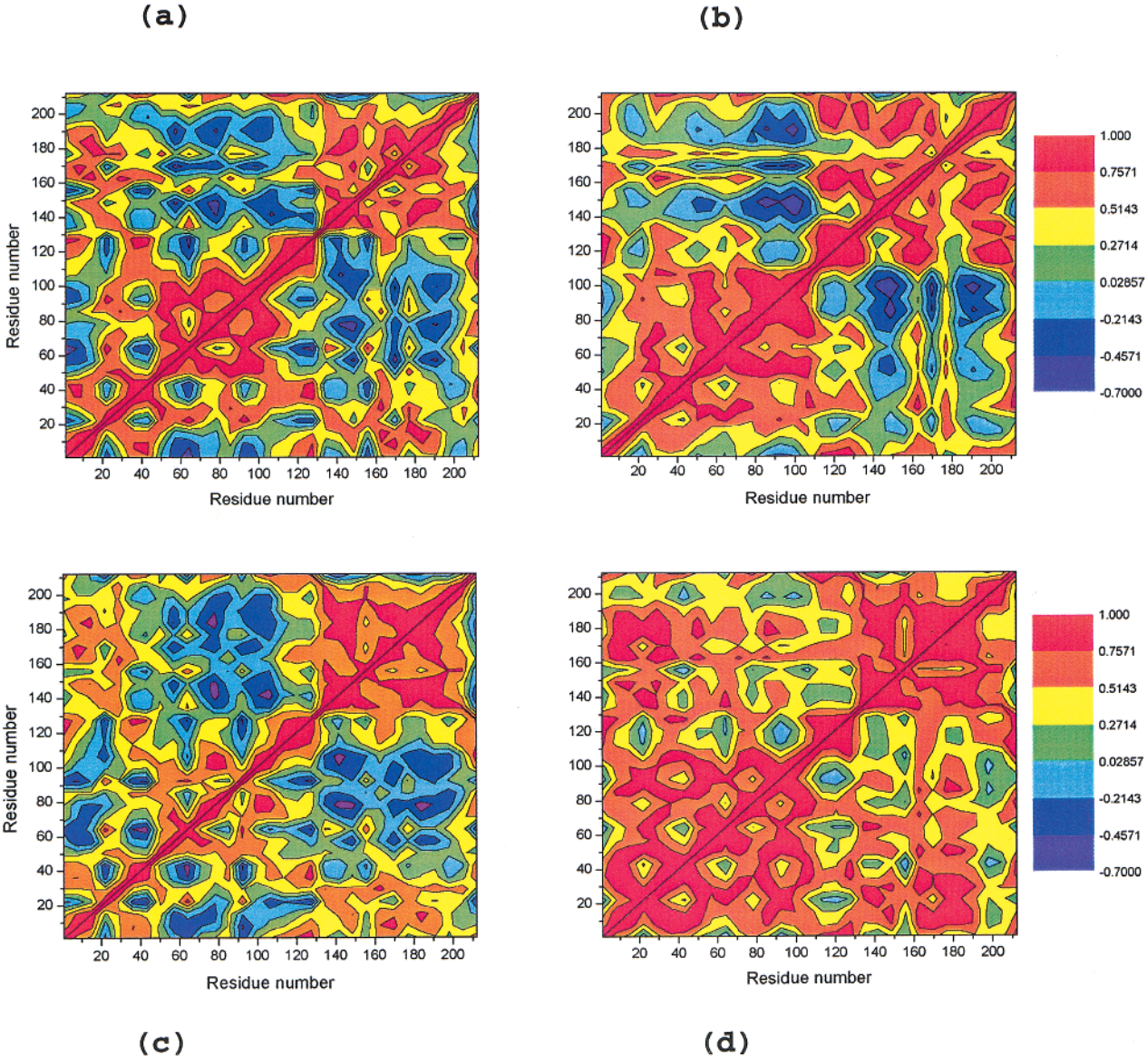

Figure 11. Cross-correlation of residue−residue fluctuations of the C_α atom of MD structures of (a) wild-type and (b) mutant papain−peptide nitrile complexes of **I** averaged for 451−1500 ps and mutant enzyme covalent intermediates (c) thioimidate **II** and (d) protonated thioimidate **III** averaged for 226−1000 ps. The range of correlations is indicated by the various colors of the panel.

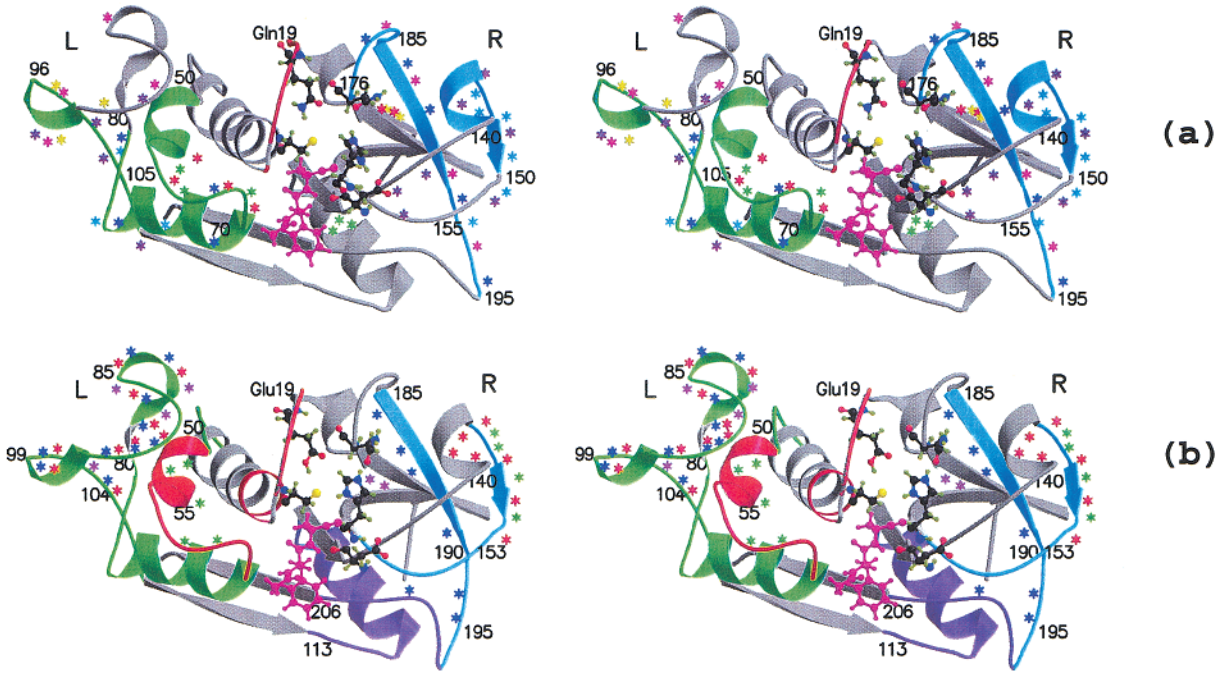

Figure 12. Mapping of the correlated motions in L and R domains of the averaged (451−1500 ps) MD structures of (a) wild-type and (b) mutant enzyme−substrate **I** complexes. Ball and stick representation is used for the active site residues Cys25, Asp158, His159, Asn175, and Gln19/Glu19. The thiolate is in yellow, and the substrate is in magenta. The positive-correlated motions among residues are represented by the same color. Residues with no significant positive-correlated motions are displayed in gray and those with strong anticorrelations are designated by the same colored stars.

papain·**I** complex are due to coupled motions among residues 60−100 of L domain and residues 155−170 of R domain (Figure 11b). No significant correlations are noticed in the stretch of residues 17−27 of the L domain that constitutes the reactive residues 19 and 25 of the active site.

Covariance analysis of C_α fluctuations indicates that anticorrelated motions occur at sites of interactions among interdomain residues in wild-type and mutant papain·**I** complexes (Figure 12). Most predominant negative correlations (shown by violet color) are associated with interactions of nonhelical residues 140−155 and 185−200 of the R domain coupled with L domain residues 75−100. The latter stretch relates to residues of the α-helix that may be involved in substrate binding between the L and R domains. A comparison between wild-type and mutant enzyme·**I** complexes (Figures 11a and 11b) indicates that positive and negative correlations are extended in the latter structure.

The pattern of negative correlations noticed in simulation of mutant enzyme·**II** covalent intermediate (Figure 11c) is similar to mutant enzyme·**I** complex (Figure 11b). However, the magnitude of these correlations in intermediate **II** is lower by a factor of 0.1−0.3. Anticorrelations are inconspicuous in mutant enzyme·**III** covalent intermediate (Figure 11d).

Conclusions

The Gln19Glu mutant papain hydrolyzes peptide substrates with terminal $-CONH_2$ replaced by $-CN$.[13] In the amidase and nitrilase activities, Cys25$-S^-$ carries out nucleophilic additions upon the carbons of $-C(=O)NH_2$ and $-CN$, respectively. In these nucleophilic additions, His159$-ImH^+$ serves as a proton source to provide the tetrahedral covalent adduct [$-S-(OH)C(NH_2)-$peptide] and thioimidate covalent adduct [$-S-C(=NH)-$peptide], respectively. The tetrahedral intermediate collapses to the amide [peptide$-C(=O)-NH_2$], which then undergoes hydrolysis by papain while the thermodynamically unstable thioimidate reverts back to the substrate and papain. The nitrile hydratase activity of the Gln19Glu mutant arises from the ability of Glu19$-CO_2H$ to donate a proton to the thioimidate covalent adduct to provide [$-S-C(=NH_2^+)-$peptide], which is thermodynamically stable and undergoes hydrolysis via the same tetrahedral intermediate formed from papain and amide substrate. The hydrolysis of nitrile peptide **I** by the Glu19$-CO_2H$ mutant exceeds that for papain nitrile hydrolysis by 4×10^5 fold.[13] The reaction has now been investigated with enzyme in aqueous solution employing nanosecond MD simulations. The systems thus investigated are: (1) the peptide nitrile substrate (**I**) at the active sites of both papain and Gln19Glu mutant papain and (2) mutant enzyme with covalent thioimidate (**II**) and protonated thioimidate (**III**) at the active site. MD simulations of mutant·**I**, mutant·**II**, and mutant·**III** reach equilibrium and proceed to completion without undue change at the active site. The MD structure of wild-type·**I** complex resembles closely that of mutant·**I** until 405 ps, when a rotation of the imidazole moiety of His159 brings about a change in the wild-type active site. This change does not occur in mutant·**I** complex. The MD simulations lead to stable trajectories of reasonable rmsd values, 1.45−1.57 Å for wild-type and mutant complexes with **I** and 1.20−1.37 Å for enzyme-bound covalent intermediates **II** and **III**. Structures of mutant papain complexed to **I**−**III** are provided in some detail.

The important structural features that accompany nitrile (**I**) hydrolysis can best be appreciated by examination of stereo presentations of structures. Figure 3a shows the averaged MD-simulated structure of the active site of mutant·**I** complex. His159$-ImH^+$ exists as a coplanar ion pair with Cys25$-S^-$. This Cys25$-S^-\cdots$His159$-$ND1 ion pair is predominant throughout the MD simulation with the thiolate moiety at an average

distance to the nitrile carbon of 3.7 Å and the His159−ImH^+ protonated ND1 at 4.4 Å from the nitrile nitrogen. Conformers in which Cys25−S^- and nitrile carbon are at a van der Waals separation (3.42 Å) while the His159−ImH^+ and nitrile nitrogen are at a hydrogen bonding distance (Figure 3b) are present to ∼1 mol %. From this, general acid catalysis by His−ImH^+ of the nucleophilic addition of thiolate to nitrile takes place to provide mutant·**II** intermediate. In both the average and the MD structure satisfying NAC criteria of mutant·**I**, the carboxyl function of Glu19−CO_2H is ∼7 Å from the nitrile nitrogen. Upon thiolate addition and protonation by His159, this nitrogen becomes that of the thioimide product mutant·**II**. In the next step of the reaction, the thioimide nitrogen of mutant·**II** is protonated by Glu19−CO_2H. Examination of the averaged structure of the active site of mutant·**II** (Figure 9a) shows that the substrate entity has penetrated further into the active site such that the Glu19−CO_2H is, on average, at 3.75 Å from thioimide nitrogen. By MD observation, the electrostatic interaction Glu19−CO_2H···N(H)═C(peptide)−S−R is rather weak. Proton transfer provides the much more stable Glu19−CO_2^-···HN(H)═C(peptide)−S−R. Conformers in which the Glu19−CO_2H···N(H)═C− distance is less than 3.0 Å (Figure 9b) are present in 10 mol % of conformers. These observations support Glu19−CO_2H trapping of the unstable thioimide (**II**) by proton transfer to provide mutant·**III** intermediate.

Strong anticorrelations reflect interdomain interactions, characteristic of both papain peptide−nitrile **I** complexes and enzyme covalent thioimidate intermediate **II**.

Acknowledgment. Many thanks to Drs. E. Lau, M. Crowley, and D. Frederik for helpful suggestions. This work was supported by funds from the NSF (MCB-9727937) and the NIH (5R37DK0917136). The authors acknowledge computer time on UCSB's SGI Origin 2000 and at NPACI (San Diego Supercomputer Center).

Supporting Information Available: Figures S1 (time-dependent variation of dihedral angle $C_\alpha-C_\beta-C_\gamma-C_\delta$ of His159), S2 (time-dependent variations of OD1(Asn175)···NE2(His159), angle OD1(Asn175)···NE2(His159)−CG(His159), and OD1-(Asp158)···ND1(His159)), and S3 (time-dependent variations of S^-(Cys25)···CN of papain·**I** complexes). This material is available free of charge via the Internet at http://pubs.acs.org.

JA020918L